Asian Journal of Chemistry; Vol. 35, No. 9 (2023), 2085-2091

ASIAN JOURNAL OF CHEMISTRY

https://doi.org/10.14233/ajchem.2023.28050

Electrochemical Performance of Flower-like ZnO Nanostructure Crystal for Supercapacitor Electrode Applications

S. NELSON AMIRTHARAJ[1,2,*], M. MARIAPPAN[2] and V. BEAULA PREMAVATHI[1]

[1]Department of Chemistry, T.B.M.L. College (Affiliated to Bharathidasan University), Porayar-609307, India
[2]Department of Chemistry, Thiru. Vi. Ka. Government Arts College (Affiliated to Bharathidasan University), Thiruvarur-610003, India

*Corresponding author: E-mail: nelsonamirtharajs@gmail.com

Received: 22 May 2023; *Accepted*: 26 June 2023; *Published online*: 31 August 2023; AJC-21347

A straightforward, easy and low-cost process using cetyltrimethylammonium bromide (CTAB) as a templated sonochemical production method was used to prepare ZnO nanostructures with the appearance of flowers. The morphological characteristics of ZnO materials have a more significant impact on variables like the CTAB template and sonochemical reaction time. The advantage of the flower-like ZnO materials is the more active reaction centre, which improves redox processes and results in outstanding electrochemical attributes like greater specific capacitance, excellent rate capability and better cyclic stability. The specific capacitance of the flower-shaped ZnO nanostructures (ZnO-2) from the cyclic voltammetric (CV) analysis was found to be 425 F g^{-1} at a scan rate of 5 mV s^{-1} and the charge/discharge study renders the specific capacitance is 426 F g^{-1} at a current density of 1 Ag^{-1}. After 3000 CV cycles at a scan rate of 100 mV s^{-1}, 89% of the initial capacitance still was retained in the long-term cyclic stability analysis. The distinctive flower-like ZnO nanostructures can be extended more for supercapacitor device applications.

Keywords: Sonochemical, Cetyltrimethylammonium bromide, Flower-like ZnO, Supercapacitors, Energy storage.

INTRODUCTION

Flower-like ZnO nanostructures were synthesized by a simple, inexpensive cetyltrimethylammonium bromide (CTAB) templated sonochemical production technique. To this point, a number of different transition metal oxides have been shown to be suitable for use as electrode material in pseudocapacitors [1]. It is generally acknowledged that ruthenium oxide (RuO_2) is the principal active ingredient for the application of pseudocapacitor electrodes [2,3], which is due to the high specific capacitance, excellent conducting characteristics and greater environmental sustainability. The restricted accessibility and inherent toxicity of this substance have significantly restricted its utilization in commercial contexts, notwithstanding its relatively high cost. As a result, a lot of work has gone into developing different transition metal oxides such as MnO_2 [4], MoO_3 [5], SnO_2 [6], NiO [7], Co_3O_4 [8], ZnO [9] and V_2O_5 [10] materials.

Recently, ZnO has gained great interest in the area of energy storage devices, particularly supercapacitors [11,12]. Similarly, ZnO has excellent characteristics like wurtzite crystal structure, wide and direct bandgap, better binding energy (60 meV), optical, electrical, semiconductor and piezoelectric nature. ZnO has several benefits, including its availability, relatively inexpensive, low toxicity and eco-friendliness [13,14]. These characteristics and benefits of ZnO make it a desirable substance for a variety of uses such as solar cells [15,16], light-emitting diodes [17,18], photovoltaic applications [19], solar water splitting [20] and photocatalysis [21].

As a result of its exceptional characteristics and electrical conductivity, ZnO is a substance of significant concern for supercapacitor applications. For instance, Lee *et al.* [13] prepared various ZnO nanostructures through the chemical co-precipitation method and demonstrated their usage in electrochemical supercapacitor electrode application and showing the specific capacitance of 2.75 F g^{-1}. Huang *et al.* [14] demonstrated the synthesis of ZnO microspheres from metal organic framework, which exhibits the specific capacitance of 1017.5 F g^{-1} at a current density of 5 Ag^{-1}. Bishwakarma & Das [22] synthesized ZnO nanoparticles through a hybrid machining process and

examined their supercapacitor properties. It delivered 708. 75 F g^{-1} at a current density of 1 Ag^{-1} and it brought back 90.42 % initial capacitance. Saranya & Selladurai [23] reported self-assembled flower-like mesoporous ZnO nanoflakes using the hydrothermal method, which delivers 322 F g^{-1} at a scan rate of 5 mV s^{-1}.

In this endeavour, we demonstrate a simple and versatile synthetic approach to prepare ZnO flowers and it is utilized as a supercapacitor electrode material. The cetyltrimethylammonium bromide (CTAB) template was employed to alter the morphology of the ZnO materials. The X-ray diffraction (XRD) and Fourier transform infrared spectroscopy (FTIR) were used to analyze the crystalline structure and bonding properties of the ZnO materials. The supercapacitor characteristics of freshly synthesized ZnO flowers were analyzed through cyclic voltammetric, galvanostatic charge/discharge studies.

EXPERIMENTAL

All the chemicals and reagents were of an analytical grade and used as such. Zinc nitrate hexahydrate ($Zn(NO_3)_2{\cdot}6H_2O$), polyvinylidene difluoride (PVDF), carbon black and N-methyl-2-pyrrolidone. Cetyltrimethylammonium bromide (CTAB) was purchased from SRL (India). The other chemicals such as potassium hydroxide, sodium hydroxide and stainless-steel foil were purchased from Sigma-Aldrich, India.

Synthesis of ZnO material: The ZnO material was synthesized using a CTAB-assisted sonochemical synthetic approach followed by the calcination process. In a distinct preparation, 0.01 M of CTAB dissolved in 100 mL of distilled water was mixed with 0.5 M of zinc nitrate hexahydrate followed by the addition of CTAB solution and stirred for 0.5 h. In this precursor mixture, the precipitating agent such as 10 mL of 2 M NaOH, was added to it and the mixture was stirred for 20 min to obtain the precipitation. The precipitate was then transferred to the ultrasonic bath and sonicated for 40 min. The resulting precipitates were collected through centrifugation, then washed thoroughly with ethanol and deionized water, respectively at 80 ºC for 10 h and then annealed at 300 ºC for 5 h to obtain the final samples. The sonication time was varied to 0, 20 and 40 min to obtain ZnO-1, ZnO-2 and ZnO-3 samples.

Preparation of electrodes for supercapacitor analysis: In order to investigate the electrochemical properties of super capacitance, cyclic voltammetry and galvanostatic charge/discharge studies were carried out in a 1 M solution of KOH. In order to analyze the electrochemical properties, the three-electrode arrangement was employed. The saturated calomel electrode, platinum foil and ZnO coated steel foil current collector were utilized as reference counter and working electrodes, respectively. The working electrode was made using the following procedure: active material, carbon black and poly (vinylidene fluoride) (80:10:10) were ground with N-methyl-2-pyrrolidone (NMP) in a mortar and pestle. The stainless steel foil was covered with the slurry and dried in a vacuum oven at 80 ºC for 10 h. The slurry was applied to the stainless-steel foil, which was then dried in a vacuum oven at 80 ºC for 10 h. The resulting electrodes were used for supercapacitor study analysis. The weight of the active substance that was contained within the electrode materials was 4 mg.

RESULTS AND DISCUSSION

XRD studies: The material phase and crystalline nature of freshly synthesized ZnO materials were evaluated utilizing X-ray diffraction analysis and the corresponding results are displayed in Fig. 1. The sharp and high-intensity peaks are perfectly visible in all the XRD spectrum confirmed that the high crystalline nature of the ZnO materials. The diffraction peaks at 31.8º, 34.5º, 36.3º, 47.6º, 56.7º, 63.0º, 66.5º, 68.1º, 69.2º, 72.7º and 77.1º correspond to (100), (002), (101), (102), (110), (103), (200), (112), (201), (004) and (202) planes, respectively. The obtained planes are confirmed the formation of wurtzite hexagonal type ZnO structure with a space group of *P*63*mc* and it is more consistent with the JCPDS card No. 01-075-0576. The wurtzite type of hexagonal structure is more stable when compared with the zinc blende structure, which gives additional stability during the electrochemical cyclic stability analysis.

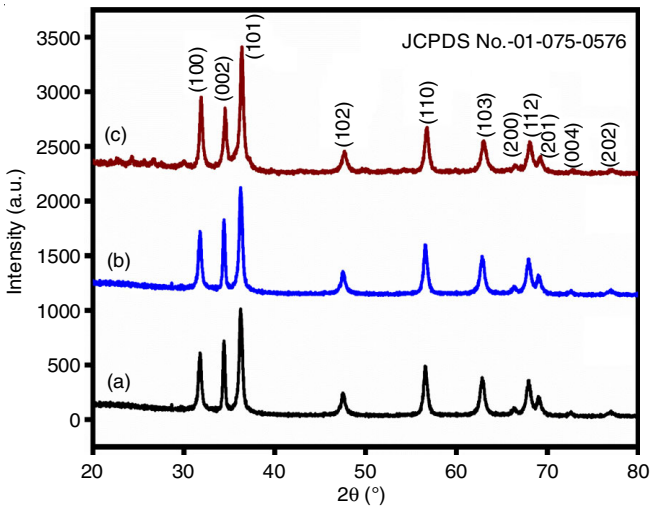

Fig. 1. XRD spectra of (a) ZnO-1; (b) ZnO-2 and (c) ZnO-3 electrode materials

FTIR studies: The FTIR analysis of the ZnO materials synthesized by the CTAB assisted sonochemical method is shown in Fig. 2. The peaks visible from 1000 to 400 cm^{-1} correspond to metal oxide peaks, which confirms the formation of ZnO materials [14,22]. The peaks at 572, 507 and 428 cm^{-1}, which are signatures of polar stretching vibrations and corresponds to E1(TO), A1(LO) and E1(LO) modes, respectively. The above mentioned three peaks signify the formation of ZnO materials [24]. The presence of the CH_2 group and the C-O-H bending mode, respectively, can be correlated to the peaks at 1325 and 1023 cm^{-1}, both of which originate from the CTAB template. The peaks at 3432 and 1621 cm^{-1} are ascribed, respectively, to stretching and bending vibrations of the O-H group [25]. The FTIR and XRD pattern results signify the formation ZnO structure.

Morphological studies: The surface textural features of ZnO materials were evaluated by HR-SEM analysis. Fig. 3a-b show lower and higher magnification HR-SEM images of ZnO-1 material, respectively. The nanoplate structure is perfectly visible in both higher and lower magnification images. The breadth and size of the nanoplates were 350 ±10 nm and 60 ±

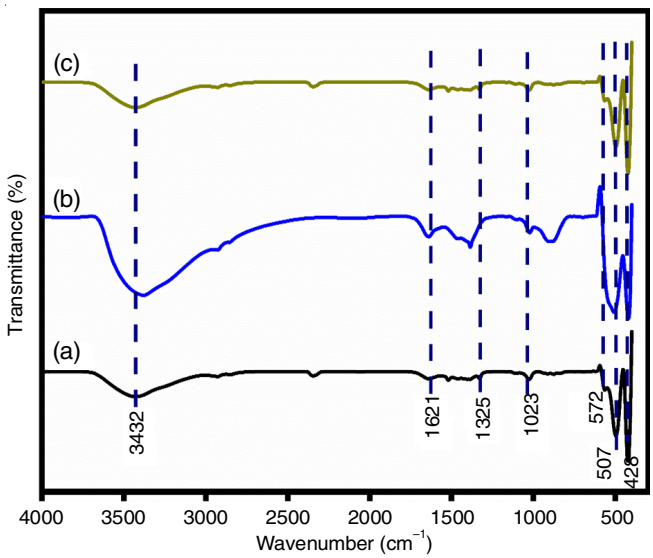

Fig. 2. FTIR spectra of (a) ZnO-1; (b) ZnO-2 and (c) ZnO-3 electrode materials

10 nm, respectively. The homogeneous formation of small nanomaterials on the surface of nanoplates is a fascinating phenomenon. The ZnO flowers (ZnO-2) are formed when increasing ultrasound irradiation time to 20 min as displayed in Fig. 3c-d. The nanoplates are combined themselves and form flower-like structural morphologies. With the increase of irradiation time to 40 min (ZnO-3), the size of the ZnO flower is increased as shown in Fig. 3e-f. When the ultrasound irradiation time was increased from 20 to 40 min, a greater number of nanoplates aggregate and manifest as micro-sized flowers. The surface analysis signifies that the template and ultrasound irradiation time has influenced more during the material generation and provides ZnO flowers.

Electrochemical studies: Various electrochemical analysis such as cyclic voltammetry (CV), cyclic stability and galvanostatic charge/discharge (CP) analysis were executed on a three-electrode set-up, employing 1 M KOH aqueous phase as the electrolyte to assess the performance of ZnO samples for supercapacitor electrode purposes. The CV analysis was recorded at various scan rates ranging from 5 to 100 mV s^{-1} within a potential range of 0-0.5 (Fig. 4a-c). These methods are commonly used to investigate the oxidation/reduction activity of processed electroactive material as well as their unique capacitive characteristics. Interestingly, during the cathodic and anodic sweeps of CV examination, a couple of well redox peaks are generated, demonstrating the pseudocapacitive character of the prepared ZnO electroactive material. The generated pair of redox peaks are attributed to valence state changes related to the Zn(II)/Zn(III) transition arisen on the surface of ZnO electrodes [26]. It should be highlighted that the redox peak potential of several prepared ZnO materials varied, which may be due to the presence of distinct surface morphological characteristics [27].

The cathodic and anodic peak potentials and peak currents for all ZnO electrodes raised with increasing scan rate, signifying diffusion-controlled reaction kinetics and faster electronic and ionic transport at the interface of electrolyte and electrode materials [23]. In addition to this, the scan rate capability of the ZnO electrode was examined using scan rates ranging from 5 to 100 mV s^{-1}. The observation that well-defined redox peaks can be observed even at faster scan rates indicates that prepared

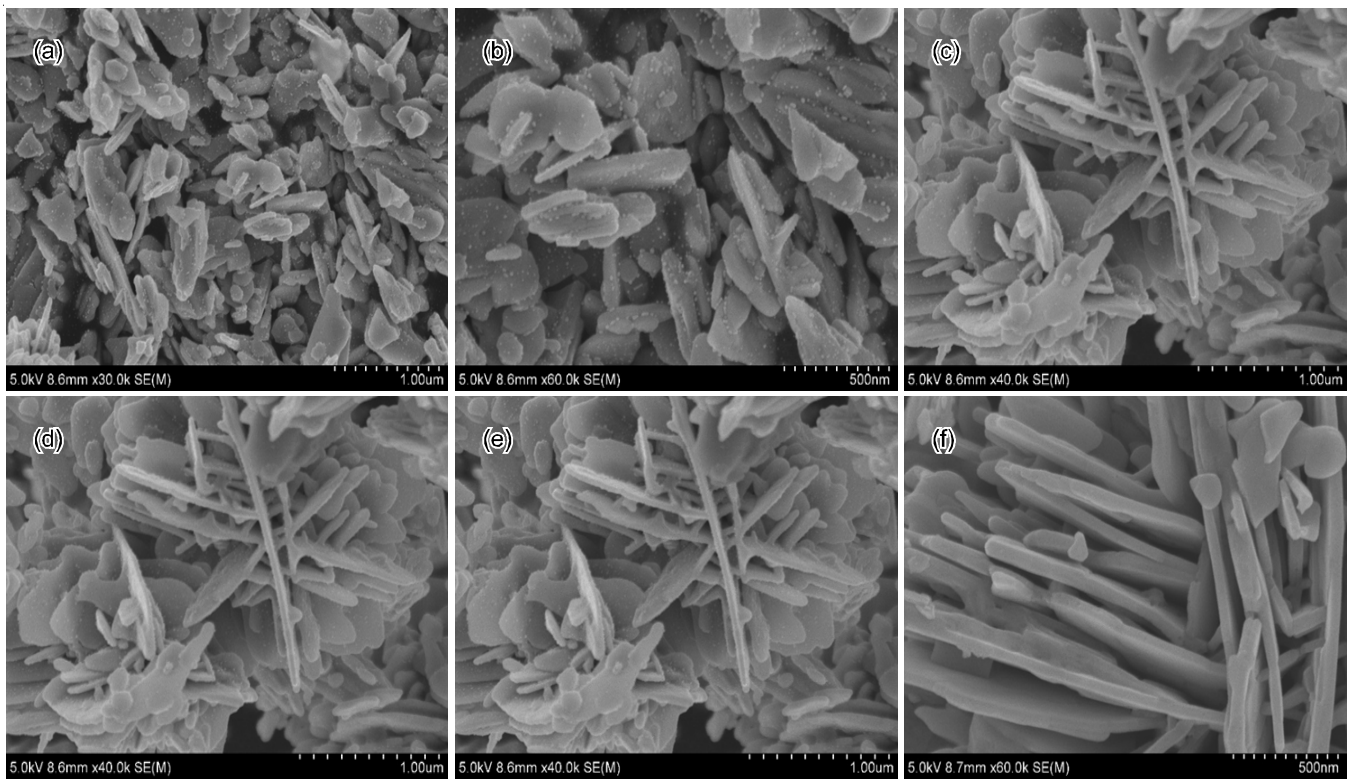

Fig. 3. Lower and higher magnification HR-SEM images of ZnO-1 (a-b) ZnO-2 (c-d) and ZnO-3 (e-f) electrode materials

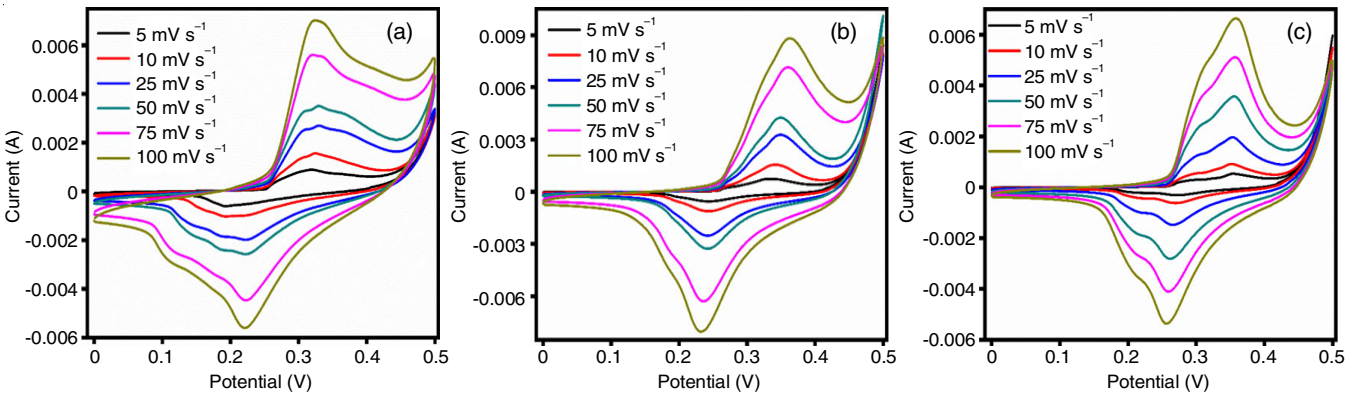

Fig. 4. Cyclic voltammetric (CV) curves of (a) ZnO-1, (b) ZnO-2, (c) ZnO-3 electrode materials

ZnO specimens are resistant to fast redox reactions. The unique capacitance character is directly proportional to the area that lies below the CV curve of active materials. Interestingly, the ZnO-2 electrode has a larger area under the CV curve than the ZnO-1 and ZnO-3 electrodes, showing that ZnO-2 electrode possess a superior capacitive property. In order to calculate specific capacitance of CV curves, eqn. 1 is used.

$$Cs = \frac{\int idV}{2 \times S \times M \times V} \quad (1)$$

where Cs is the specific capacitance (F g^{-1}); ∫idV is the integrated area of CV curves; S is the scan rate (mV s^{-1}); M is the active mass (g) and V is the potential window (V). The ZnO-1, ZnO-2 and ZnO-3 electrodes deliver the specific capacitance of 257, 425 and 329 F g^{-1}, respectively. Among all the ZnO materials, ZnO-2 provides superior capacitance than ZnO-1 and ZnO-3 materials. Fig. 5 shows that the scan rate *vs*. specific capacitance graph. It is apparent that the specific capacitance increases with the increase of scan rate from 5 to 100 mV s^{-1}. The observation that real capacitance lowers with rising current density may be attributed to low electrolyte ion diffusion on electrode surfaces. At high scan rates, only the external surface region of the electrode materials is included in the electrochemical phase, limiting the electroactive substance usage, while at lower current densities, there might be enough time for a redox reaction to proceed both in the inner and outer surface regions of the electrode substance, allowing for greater

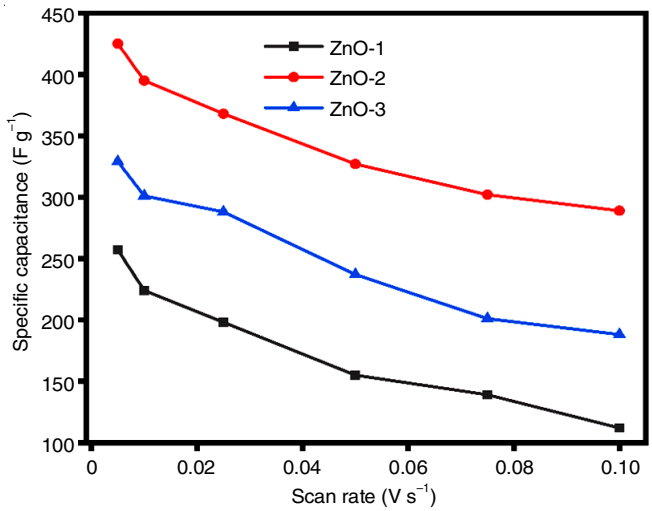

Fig. 5. Specific capacitance *vs.* scan rate graph of ZnO electrode materials

electroactive substance utilization [28]. The galvanostatic charge/discharge analysis was recorded for ZnO materials across voltage ranges of 0 to 0.45 V at different current densities of 1, 2, 3, 10 and 30 Ag^{-1} (Fig. 6a-c). All the charge-discharge current deviate significantly from a rectangular behaviour and show the non-linear profile, demonstrating that the capacitive activity is caused by a Faradic redox reaction [29]. The fact that all of the charge/discharge curves have small iR lass means that ZnO materials have good capacitive features.

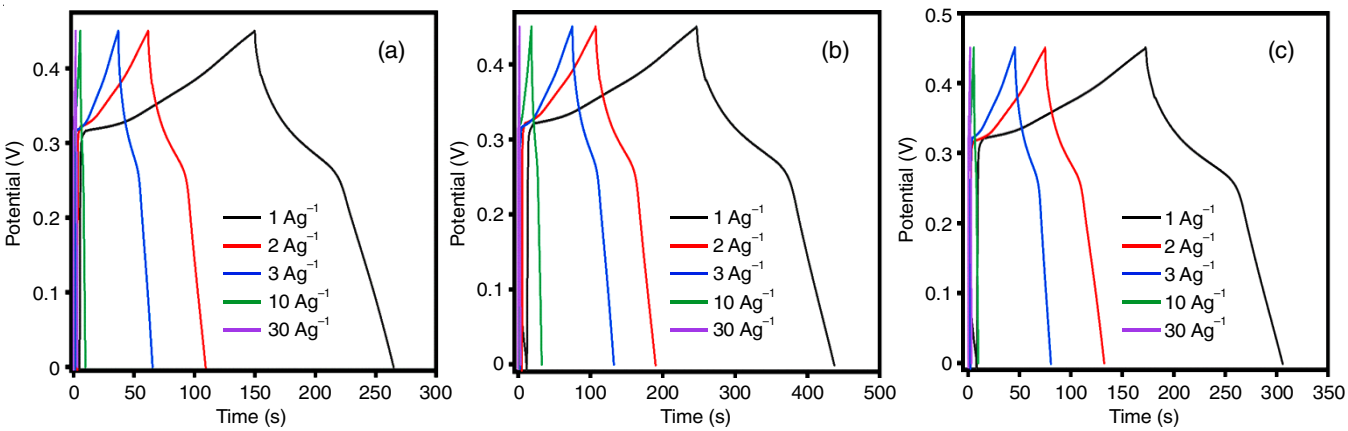

Fig. 6. Galvanostatic charge-discharge (GCD) curves of (a) ZnO-1, (b) ZnO-2, (c) ZnO-3 electrode materials

The charge/discharge curve of the ZnO-2 electrode has a longer duration compared to the other electrodes, ZnO-1 and ZnO-3. This trend supports the high specific capacitance behaviour of ZnO-2 electrode. The specific capacitance is calculated from charge/discharge curves using eqn. 2:

$$Cs = \frac{I\Delta t}{m\Delta V} \quad (2)$$

where I, Δt, m and ΔV represent the current density (Ag^{-1}), discharge time (s), the mass of active materials and the potential window. At a current density of 1 Ag^{-1}, the calculated specific capacitance values were 255, 426 and 307 F g^{-1} for ZnO-1, ZnO-2 and ZnO-3 electrodes, respectively. The higher specific capacitance values were due to the flower-like nanostructure of the current ZnO-2 electrode material, which contributes to good electrolyte penetration, resulting in shorter OH^- ion diffusion time and more usable spaces for redox reactions. Furthermore, The ZnO flowers, which are made up of centrifugally self-assembled nanoplates, can significantly improve the electrode/electrolyte contact area and speed up electron and ion movement. Since every plate is in interaction with the electrolyte, the open space between the neighbouring plates allows for quick diffusion of the electrolyte, ensuring that each sheet can contribute to the electrochemical process. The ZnO-3 materials deliver lower capacitance when compared with ZnO-2 materials, which due to the larger size ZnO flower structure and the small gap between neighborhood plates, restricts the ion transport and it reduced the specific capacitance.

When the density of the current is low, the capacitance is high, but as the density of the current rises, the capacitance decreases gradually (Fig. 7). The drop in capacitance is primarily due to a decrease in voltage drop in discharge curves as current density increases, as well as slow reaction kinetics at the interface of electrolyte/electrode materials. The energy density and power density parameters of supercapacitors are extremely significant for device fabrication. The charge/discharge profiles can be utilized to calculate energy and power densities, which are calculated using eqns. 3 and 4:

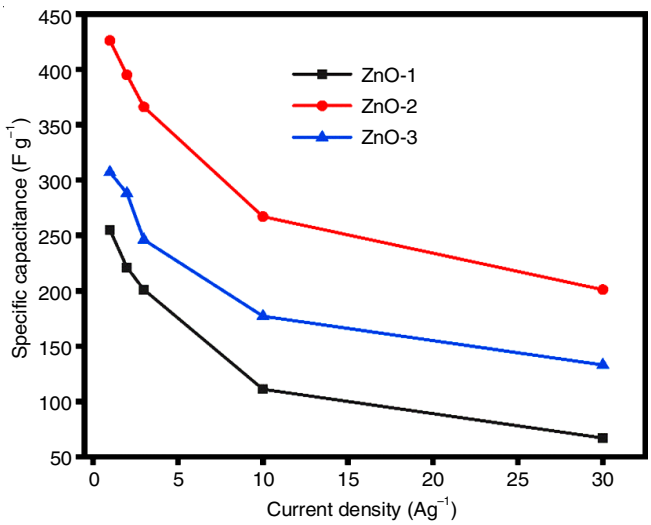

Fig. 7. Specific capacitance *vs*. current density graphs of ZnO electrode materials

$$E = \frac{1}{2}\frac{C \times V^2}{3.6} \quad (3)$$

$$P = \frac{E \times 3600}{t} \quad (4)$$

where E, C, V, P and t represent energy density (Wh Kg^{-1}), specific capacitance (F g^{-1}), potential window (V), power density (W Kg^{-1}) and discharge time, respectively. The relationship between energy density and power density is shown in Fig. 8. The ZnO-1, ZnO-2 and ZnO-3 electode materials obtained the energy densities of 7, 12 and 8.6 Wh Kg^{-1}, respectively. Additionally, ZnO-1, ZnO-2 and ZnO-3 electrodes, respectively, produced power density values of 3600, 6720 and 6660 W Kg^{-1}. The flower structure of ZnO-2 electrodes gives them higher energy and power densities than ZnO-1 and ZnO-3 electrode materials due to their unique morphological properties.

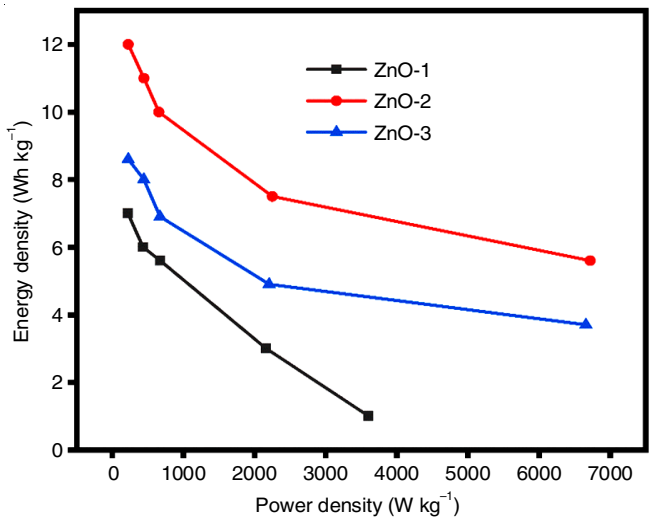

Fig. 8. Energy density *vs*. power density of ZnO-1; ZnO-2 and ZnO-3 electrode materials

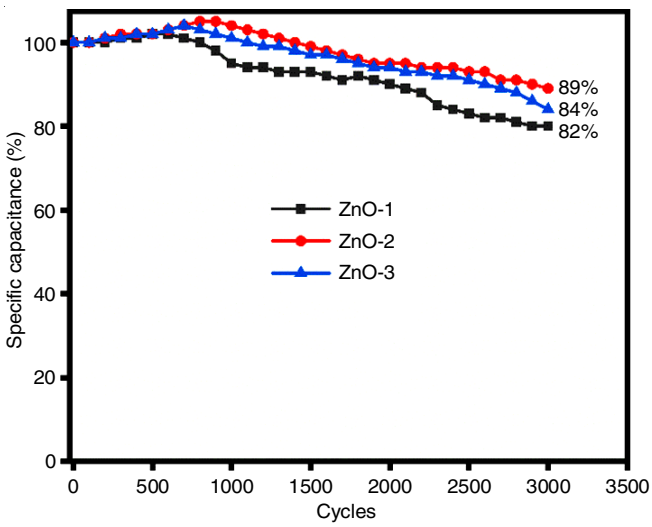

Fig. 9. Cyclic stability studies of (a) ZnO-1, (b) ZnO-2 and (c) ZnO-3 electrode materials

The cycling stability is very important for supercapacitors and this is tested by 3000 continuous CV cycles at a scanning

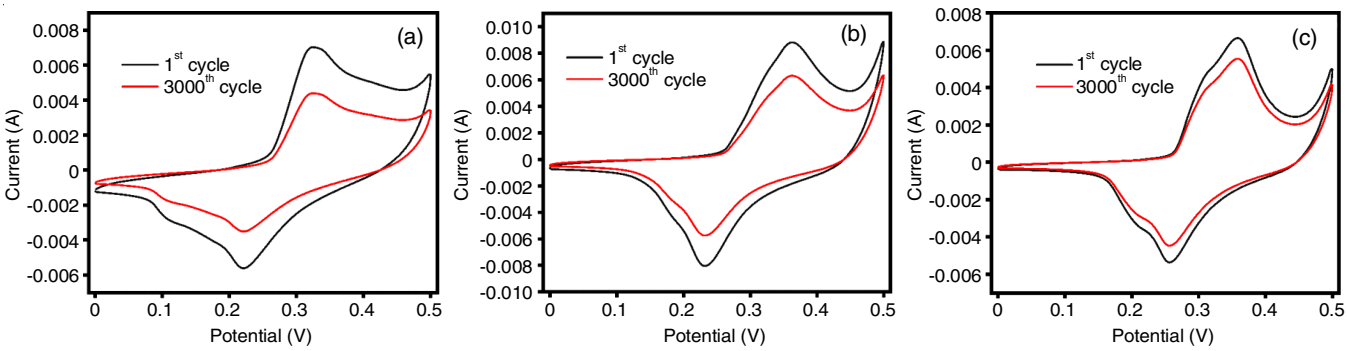

Fig. 10. 1st and 3000th cycles of cyclic stability studies for (a) ZnO-1, (b) ZnO-2, (c) ZnO-3 material

rate of 100 mV s^{-1}. The studies of the ZnO-1, ZnO-2 and ZnO-3 electrodes' cyclic stability are shown in Fig. 9. Fig. 10 show the 1st and 3000th cycles of cyclic stability studies for ZnO-1, ZnO-2 and ZnO-3, respectively. It can be shown that the preliminary specific capacitance increases steadily over 800 cycles, which can be due to the complete activation process of the current ZnO electrodes [30]. After that the specific capacitances are steadily decreased until they are able to withstand 80% (ZnO-1), 89% (ZnO-2) and 84% (ZnO-3) of their initial capacitance after 3000 successive cycles. The fact that the ZnO-2 electrode has better cyclic stability than the ZnO-1 and ZnO-3 electrodes, which implies that ZnO-2 flowers are more advantageous than other morphologies for improving the electrochemical efficiency.

Conclusion

A facile, cetyltrimethylammonium bromide (CTAB) assisted sonochemical approach was followed to generate flower-like ZnO nanostructures. The factors such as CTAB template and sonochemical reaction time are more influenced by the morphological properties of ZnO materials. The synthetic approach is simple and cost-effective. The more active reaction center is the beneficial feature of flower-like ZnO materials, which provide better redox reactions leading to phenomenal electrochemical properties such as high specific capacitance, good rate capability and enhanced cyclic stability. The CV analysis of flower-like ZnO nanostructures (ZnO-2) yields a specific capacitance of 425 F g^{-1} at a scan rate of 5 mV s^{-1}, whereas the charge/discharge investigation yields a specific capacitance of 426 F g^{-1} at a current density of 1 Ag^{-1}. After 3000 CV cycles at a scan rate of 100 mV s^{-1}, 89 % of the initial capacitance was preserved in a long-term cyclic stability analysis. The flower-like ZnO nanostructures can be further expanded for the supercapacitor device applications.

CONFLICT OF INTEREST

The authors declare that there is no conflict of interests regarding the publication of this article.

REFERENCES

1. S.A. Delbari, L.S. Ghadimi, R. Hadi, S. Farhoudian, A. Babapoor, A.S. Namini, M. Nedaei, Q.V. Le, M. Shokouhimehr, M. Mohammadi and M.S. Asl, *J. Alloys Comp.*, **857**, 158281 (2021); https://doi.org/10.1016/j.jallcom.2020.158281
2. C.C. Hu, K.H. Chang, M.C. Lin and Y.T. Wu, *Nano Lett.*, **6**, 2690 (2006); https://doi.org/10.1021/nl061576a
3. V. Subramanian, S.C. Hall, P.H. Smith and B. Rambabu, *Solid State Ion.*, **175**, 511 (2004); https://doi.org/10.1016/j.ssi.2004.01.070
4. S. Zhao, T. Liu, D. Hou, W. Zeng, B. Miao, S. Hussain, X. Peng and M.S. Javed, *Appl. Surf. Sci.*, **356**, 259 (2015); https://doi.org/10.1016/j.apsusc.2015.08.037
5. G.D. Jeyaleela, J.R. Vimala, S.M. Sheela, A. Agila, M.S. Bharathy and M. Divya, *Orient. J. Chem.*, **36**, 655 (2020); https://doi.org/10.13005/ojc/360409
6. V. Bonu, B. Gupta, S. Chandra, A. Das, S. Dhara and A.K. Tyagi, *Electrochim. Acta*, **203**, 230 (2016); https://doi.org/10.1016/j.electacta.2016.03.153
7. G.A. Babu, G. Ravi, T. Mahalingam, M. Kumaresavanji and Y. Hayakawa, *Dalton Trans.*, **44**, 4485 (2015); https://doi.org/10.1039/C4DT03483J
8. R. Tummala, R.K. Guduru and P.S. Mohanty, *J. Power Sources*, **209**, 44 (2012); https://doi.org/10.1016/j.jpowsour.2012.02.071
9. G. Theophil Anand, D. Renuka, R. Ramesh, L. Anandaraj, S. John Sundaram, G. Ramalingam, C.M. Magdalane, A.K.H. Bashir, M. Maaza and K. Kaviyarasu, *Surf. Interfaces*, **17**, 100376 (2019); https://doi.org/10.1016/j.surfin.2019.100376
10. J. Yang, T. Lan, J. Liu, Y. Song and M. Wei, *Electrochim. Acta*, **105**, 489 (2013); https://doi.org/10.1016/j.electacta.2013.05.023
11. T. Wei, N. Zhang, Y. Ji, J. Zhang, Y. Zhu and T. Yi, *Chinese Chem. Lett.*, **33**, 714 (2022); https://doi.org/10.1016/j.cclet.2021.06.037
12. G.M. Di Mari, G. Mineo, G. Franzò, S. Mirabella, E. Bruno and V. Strano, *Nanomaterials*, **12**, 2588 (2022); https://doi.org/10.3390/nano12152588
13. K.S. Lee, C.W. Park and J.D. Kim, *Colloids Surf. A Physicochem. Eng. Asp.*, **512**, 87 (2017); https://doi.org/10.1016/j.colsurfa.2016.10.022
14. G. Huang, W. Zhang, S. Xu, Y. Li and Y. Yang, *Ionics*, **22**, 2169 (2016); https://doi.org/10.1007/s11581-016-1745-7
15. M. Selvakumar, D.K. Bhat, A.M. Aggarwal, S.P. Iyer and G. Sravani, *Physica B*, **405**, 2286 (2010); https://doi.org/10.1016/j.physb.2010.02.028
16. X. Li, Z. Wang, Y. Qiu, Q. Pan and P. Hu, *J. Alloys Compd.*, **620**, 31 (2015); https://doi.org/10.1016/j.jallcom.2014.09.105
17. K. Keis, C. Bauer, G. Boschloo, A. Hagfeldt, K. Westermark, H. Rensmo and H. Siegbahn, *J. Photochem. Photobiol. Chem.*, **148**, 57 (2002); https://doi.org/10.1016/S1010-6030(02)00039-4
18. K. Matsubara, P. Fons, K. Iwata, A. Yamada, K. Sakurai, H. Tampo and S. Niki, *Thin Solid Films*, **431–432**, 369 (2003); https://doi.org/10.1016/S0040-6090(03)00243-8
19. B.-H. Hwang, C.-L. Chang, C.-S. Hsu and C.-Y. Fu, *J. Phys. D Appl. Phys.*, **40**, 3448 (2007); https://doi.org/10.1088/0022-3727/40/11/028
20. S.J. Pearton and F. Ren, *Curr. Opin. Chem. Eng.*, **3**, 51 (2014); https://doi.org/10.1016/j.coche.2013.11.002

21. K. Keis, L. Vayssieres, S.E. Lindquist and A. Hagfeldt, *Nanostruct. Mater.*, **12**, 487 (1999); https://doi.org/10.1016/S0965-9773(99)00165-8
22. H. Bishwakarma and A.K. Das, *J. Electron. Mater.*, **49**, 1541 (2020); https://doi.org/10.1007/s11664-019-07835-x
23. P.E. Saranya and S. Selladurai, *Int. J. Nanosci.*, **17**, 1760002 (2018); https://doi.org/10.1142/S0219581X1760002X
24. M. Faisal, S.B. Khan, M.M. Rahman, A. Jamal, A.M. Asiri and M.M. Abdullah, *Appl. Surf. Sci.*, **258**, 672 (2011); https://doi.org/10.1016/j.apsusc.2011.07.067
25. Q. Yuan, S. Hein and R.D.K. Misra, *Acta Biomater.*, **6**, 2732 (2010); https://doi.org/10.1016/j.actbio.2010.01.025
26. A. Sahai and N. Goswami, *Physica E*, **58**, 130 (2014); https://doi.org/10.1016/j.physe.2013.12.009
27. A.S. Lanje, S.J. Sharma, R.S. Ningthoujam, J.S. Ahn and R.B. Pode, *Adv. Powder Technol.*, **24**, 331 (2013); https://doi.org/10.1016/j.apt.2012.08.005
28. X. Wang, M. Li, Z. Chang, Y. Wang, B. Chen, L. Zhang and Y. Wu, *J. Electrochem. Soc.*, **162**, A1966 (2015); https://doi.org/10.1149/2.0041511jes
29. J. Zhang, H. Feng, Q. Qin, G. Zhang, Y. Cui, Z. Chai and W. Zheng, *J. Mater. Chem. A Mater. Energy Sustain.*, **4**, 6357 (2016); https://doi.org/10.1039/C6TA00397D
30. A.A. Kashale, M.M. Vadiyar, S.S. Kolekar, B.R. Sathe, J.Y. Chang, H.N. Dhakal and A.V. Ghule, *RSC Adv.*, **7**, 36886 (2017); https://doi.org/10.1039/C7RA05655A